Volume 19 | Number 12 | 28 March 2017 | Pages 8123–8622

PCCP

Physical Chemistry Chemical Physics

rsc.li/pccp

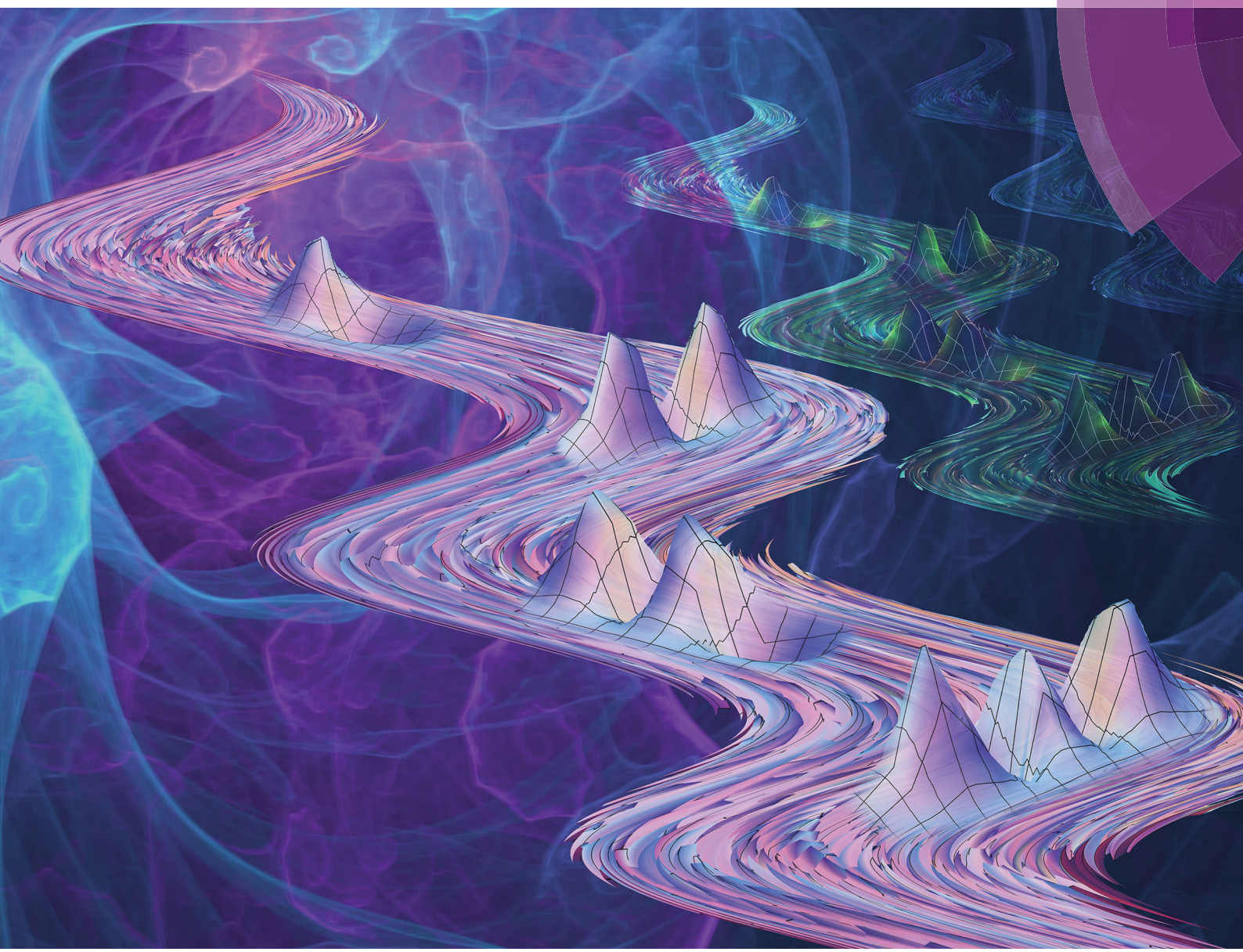

ISSN 1463-9076

ROYAL SOCIETY OF CHEMISTRY

PAPER

Attila G. Császár, Thierry Stoecklin *et al.*

Complex rovibrational dynamics of the $Ar{\cdot}NO^+$ complex

PCCP

PAPER

Cite this: *Phys. Chem. Chem. Phys.*, 2017, **19**, 8152

Complex rovibrational dynamics of the Ar·NO$^+$ complex†

Dóra Papp,[a] János Sarka,[a] Tamás Szidarovszky,[a] Attila G. Császár,*[a] Edit Mátyus,[b] Majdi Hochlaf[c] and Thierry Stoecklin*[d]

Received 11th November 2016,
Accepted 31st January 2017

DOI: 10.1039/c6cp07731e

rsc.li/pccp

Rotational–vibrational states of the Ar·NO$^+$ cationic complex are computed, below, above, and well above the complex's first dissociation energy, using variational nuclear motion and close-coupling scattering computations. The HSLH potential energy surface used in this study (*J. Chem. Phys.*, 2011, **135**, 044312) is characterized by a first dissociation energy of D_0 = 887.0 cm^{-1} and supports 200 bound vibrational states. The bound-state vibrational energies and the corresponding wave functions allow the interpretation of the scarcely available experimental results about the intermonomer vibrational motion of the complex. A very large number of long-lived quasibound combination states of the three vibrational modes, exhibiting a very similar energy-level structure as that of the bound states, are found embedded in the continuum. Additional short-lived resonance states are also identified and their properties are analyzed.

1 Introduction

Weakly-bound triatomic systems involving a strongly-bound diatomic, AB, and a rare gas atom (Rg = He, Ne, Ar, Kr) loosely attached to it[1–5] represent ideal benchmark systems to study van der Waals (vdW) interactions and unusual aspects of chemical bonding. The two-dimensional (2D) description of the vibrational dynamics based on the potential energy hypersurfaces (PES) of these Rg·AB systems is expected to be quite close to the complete, 3D description. Rg·AB complexes thus provide excellent benchmarks for the detailed study of the dynamical consequences of the adiabatic separation of the diatomic vibrational degree of freedom. The shallow well of Rg·AB complexes also provides a good opportunity to obtain benchmark results about computational algorithms determining scattering as well as highly excited bound states. At the same time, one should not forget that molecules and complexes involving rare gas atoms find application during the study of cold collisions,[6] solvation,[7] as well as in astrophysics.[8–10]

There are many possible variants of the diatomic molecule involved in Rg·AB complexes. For example, AB can be neutral or charged. Out of the expansive literature, including reviews,[1,5] for the neutral cases we mention here the He·H$_2$,[11] He·HF,[12] He·CN,[13] He·CO,[14] Ne·H$_2$,[15] Ar·N$_2$,[16,17] and Rg·halogen systems,[18–20] and in particular Ar·NO,[21–23] one of the favorite benchmarks of studies on vdW systems. If AB has a positive charge, the bonding to Rg, through stronger polarization, may become relatively strong and the first dissociation energy drastically increases, from only a few tens of cm^{-1} for neutral ABs up to several hundred cm^{-1}. This leads to a relatively large number of bound rotational–vibrational states for the ground electronic state and perhaps more interesting and involved dynamical behavior.[24,25] The charged molecular species investigated include Ar·NO$^+$,[26–37] Ar$_m$BeO^{q+},[38,39] with m = 1, 2, 3 and q = 1, 2,

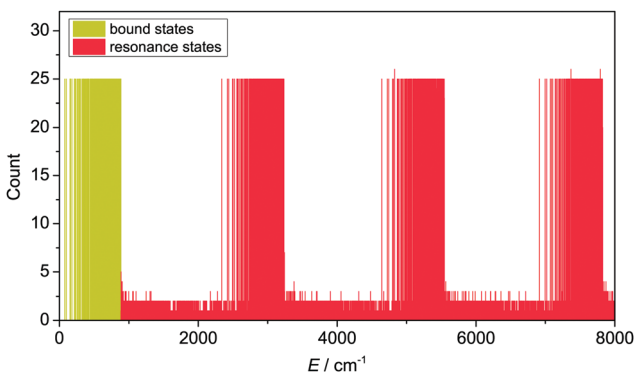

Fig. 1 Overview of the stabilization-method histogram in the 0–8000 cm^{-1} energy interval based on 25 individual GENIUSH computations.

[a] *MTA-ELTE Complex Chemical Systems Research Group, P.O. Box 32, H-1518 Budapest 112, Hungary. E-mail: csaszar@chem.elte.hu*
[b] *Institute of Chemistry, Eötvös University, Pázmány Péter sétány 1/A, H-1117 Budapest, Hungary*
[c] *Université Paris-Est, Laboratoire Modélisation et Simulation Multi Echelle, MSME UMR 8208 CNRS, 5 bd Descartes, F-77454 Marne-la-Vallée, France*
[d] *Institut des Sciences Moléculaires, Université de Bordeaux, CNRS UMR 5255, 33405 Talence Cedex, France. E-mail: thierry.stoecklin@u-bordeaux.fr*

† Electronic supplementary information (ESI) available: (a) The 2D cuts of the wave functions of all the 200 vibrational bound states of the Ar·NO$^+$ complex along the R and θ Jacobi coordinates obtained from GENIUSH computations; and (b) rovibrational (J = 0, 1 and 2) bound energy levels from GENIUSH (reduced- and full-dimensional) and close-coupling scattering computations. See DOI: 10.1039/c6cp07731e

Ar_mH^+,[40] Ar_mC^+,[41] Ar_mAu^+,[42] Ar_mHCl^+,[43,44] and $Ar_mH_5O_2^+$.[45] It is especially interesting when the dynamics of both the neutral and the (positively) charged Rg·AB systems are well understood, as this allows interpretation of results of several experimental techniques, including photoelectron, resonantly enhanced multiphoton ionization (REMPI), and infrared multiphoton dissociation (IRMPD) spectroscopies. In this paper we make a large step in the direction of a full understanding of the complex nuclear dynamics of the relatively strongly bound Ar·NO^+ charge-transfer complex both below and above the first dissociation asymptote.

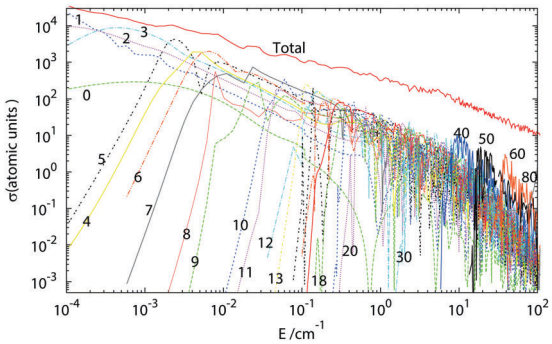

Fig. 2 Partial wave expansion of the rotational quenching cross section of NO^+ (v = 0,j = 1) in collision with Ar. Each number in the figure represents a total angular momentum quantum number J.

A dynamical study of the Ar·NO^+ complex offers several notable challenges: (1) the challenge of generating an accurate PES was met in a previous study with the participation of two of the present authors,[37] yielding the HSLH PES. A detailed discussion about the different PESs[27,29,37] available for Ar·NO^+ can be found in ref. 37. (2) Because of the shallow potential well and the low barrier to end-over-end hindered internal rotation of the monomers, Rg·AB vdW complexes are particularly floppy and exhibit large amplitude motions (LAM) upon excitation. The LAMs invalidate the use of anharmonic force fields[46] and standard vibrational perturbation theory[47,48] treatments for dynamical studies; for this class of systems variational treatments on accurate (semi)global PESs are mandatory. Variational studies started in ref. 37 are continued here. (3) Bound vibrational energy levels have been obtained for Ar·NO^+ in experimental studies.[26,33] These low-resolution results call for a thorough theoretical interpretation utilizing energies and wave functions coming from variational studies. (4) Quasi-bound rovibrational states have neither been computed nor measured for Ar·NO^+. As shown below, these states highlight interesting physical phenomena.

Since ref. 37 contains a considerable amount of computed results for the bound states of Ar·NO^+, the emphasis of the

Table 1 Comparison of the first and last 15 bound vibrational (J = 0) and rovibrational (J = 1 and 2) energy levels, given in cm^{-1}, of the Ar·NO^+ complex computed in full-dimensional (3D and 6D, the latter including the 3 rotational degrees of freedom) and reduced-dimensional (2D and 5D) models, in the latter cases the r coordinate is held fixed at its equilibrium value, using the variational GENIUSH approach and close-coupling scattering (CC) theory

	J = 0				J = 1				J = 2		
	GENIUSH		CC		GENIUSH		CC		GENIUSH		CC
No.	2D	3D		No.	5D	6D		No.	5D	6D	
1	96.62	1278.19		1	0.20	0.20	0.20	1	0.59	0.59	0.59
2	78.24	78.53	78.54	2	2.48	2.48	2.48	2	2.86	2.87	2.86
3	95.94	96.80	96.81	3	2.48	2.48	2.48	3	2.88	2.88	2.88
4	151.29	152.29	152.25	4	78.43	78.72	78.73	4	9.72	9.72	9.71
5	158.86	160.12	160.14	5	80.84	81.14	81.14	5	9.72	9.72	9.71
6	178.59	179.63	179.62	6	80.85	81.14	81.15	6	78.81	79.10	79.11
7	213.03	214.69	214.62	7	96.13	96.99	97.00	7	81.22	81.51	81.52
8	222.09	223.14	223.09	8	98.31	99.17	99.17	8	81.24	81.53	81.54
9	233.30	234.65	234.64	9	98.32	99.17	99.18	9	88.46	88.75	88.75
10	254.37	255.54	255.52	10	151.48	152.47	152.44	10	88.46	88.75	88.75
11	270.19	271.66	271.63	11	154.02	155.03	154.99	11	96.52	97.38	97.38
12	283.98	285.47	285.37	12	154.03	155.04	155.00	12	98.69	99.55	99.55
13	288.82	290.01	289.95	13	159.05	160.30	160.33	13	98.71	99.56	99.57
14	302.37	303.81	303.77	14	161.39	162.62	162.65	14	105.24	106.08	106.08
15	321.79	323.10	323.07	15	161.40	162.63	162.65	15	105.24	106.08	106.08
186	876.99	879.63	879.47	536	880.92	883.74	883.53	845	881.93	884.55	884.40
187	878.01	880.36	880.20	537	881.45	884.28	884.08	846	882.21	884.56	884.41
188	878.49	880.96	880.80	538	881.83	884.44	884.19	847	882.26	884.85	884.70
189	879.54	882.12	881.96	539	881.84	884.75	884.60	848	882.33	884.86	884.71
190	879.58	882.47	882.31	540	882.05	884.76	884.61	849	882.33	885.09	884.93
191	879.83	882.76	882.60	541	882.21	885.22	885.11	850	882.64	885.09	884.93
192	880.88	883.69	883.49	542	882.53	885.47	885.37	851	882.99	885.27	885.19
193	881.41	884.24	884.05	543	882.96	885.74	885.78	852	883.20	885.55	885.44
194	881.97	884.39	884.13	544	883.23	885.97	885.90	853	883.21	885.79	885.83
195	882.19	885.20	885.08	545	883.24	886.01	885.95	854	883.33	886.09	886.03
196	882.49	885.44	885.35	546	883.40	886.09	886.08	855	883.34	886.16	886.05
197	882.94	885.91	886.14	547	883.73	886.13	886.42	856	883.43	886.19	886.43
198	883.39	886.29	886.78	548	884.06	886.40		857	883.76	886.43	886.66
199	883.72	886.57		549	884.11	886.66		858	884.11	886.48	
200	884.08	886.84		550	884.11	886.90		859	884.16	886.78	

present study is on quasibound states above the first dissociation asymptote, $NO^+(X^1\Sigma^+)$ + Ar, using sophisticated Hermitian and non-Hermitian techniques of molecular scattering and variational nuclear motion theories.

2 Computational details

2.1 The HSLH potential energy surface

The accurate, correctly dissociating 3D HSLH PES generated in ref. 37 for the ground electronic state of $Ar{\cdot}NO^+$ is used in this study. The equilibrium structure of $Ar{\cdot}NO^+$ on the HSLH PES can be conveniently represented by the standard Jacobi coordinates, r, R, and θ, which are also used in what follows to describe the vibrational motions of the complex: r denotes the distance between the N and O atoms, R is the distance of Ar from the center of mass of the NO^+ unit, and the θ angular coordinate is the included angle of the two vectors. $Ar{\cdot}NO^+$ is an approximately T-shaped molecule with the Ar atom lying on the N side. The precise equilibrium structural parameters of the $Ar{\cdot}NO^+$ complex, calculated from the HSLH PES,[37] are r_e = 2.013377 a_0, R_e = 5.858267 a_0, and θ_e = 66.6638°. The pure electronic dissociation energy corresponding to the HSLH PES is D_e = 980.35 cm^{-1}, while the corresponding D_0 is 887.00 cm^{-1}.

2.2 Computational techniques for solving the nuclear Schrödinger equation

All nuclear-motion computations of this study utilized the orthogonal Jacobi internal coordinate system and the following masses: $m(^{14}N)$ = 14.003074 u, $m(^{16}O)$ = 15.994915 u, and $m(^{40}Ar)$ = 39.962383 u.

2.2.1 GENIUSH. The fourth-age[49] quantum chemical code GENIUSH[50,51] is employed in this study to compute the complete set of vibrational and many bound and quasibound (ro)vibrational states of $Ar{\cdot}NO^+$. GENIUSH is a general (GE) code with a numerical (N), internal-coordinate (I), user-specified (US) Hamiltonian (H), and it computes the rovibrational states of polyatomic molecules using a discrete variable representation (DVR) and an iterative Lanczos eigensolver. Reduced-dimensional models can be defined simply within GENIUSH by fixing the internal coordinates and deleting the corresponding rows and columns of the mass-weighted metric tensor.[50]

Converged bound rovibrational energy levels, even near the dissociation threshold, are obtained by using 20 and 100 Laguerre-DVR grid points for the r and R coordinates scaled to the ranges of [1.68,2.64] a_0 and [4.0,40.0] a_0, respectively. For the angular coordinate it is sufficient to employ 40 unscaled Legendre-DVR grid points for $J = 0$, where J is the rotational quantum number. However, for $J > 0$ we had to employ 100 Legendre DVR basis functions. For the $J > 0$ rovibrational computations the R embedding and a basis extended with $2J + 1$ orthonormal Wang functions is used. One- (fixed R and θ) and two- (fixed r) dimensional models are also employed to explore the coupling of the degrees of freedom of the $Ar{\cdot}NO^+$ complex; in these cases the inactive coordinates are fixed at their equilibrium values. The rovibrational states are characterized by counting the nodes of the computed wave functions and by computing expectation values of the vibrational coordinates.

To identify certain long-lived vibrational resonances of $Ar{\cdot}NO^+$, we analyzed the eigenstates beyond D_0 obtained in a series of standard GENIUSH computations with the help of the stabilization method (SM).[52–56] We use the SM technique in its simplest form and observe the stabilization of the energy using histogram binning (see Fig. 1). No attempt is made to extract lifetimes from the computations. During the SM computations the size of the basis on R changes between 80 and 120 and the end of the coordinate range covered between 30 and 50 a_0. We analyze the first 12 000 eigenstates, obtained with a Lanczos eigensolver. The stabilization (SM) histograms reported are generated with a bin size of 0.001 cm^{-1} and are based on 25 computations (this determines the count number on the vertical axis of the SM histograms). In order to have a direct comparison with the other two techniques used here to study the quasibound regime, we also performed GENIUSH computations focusing on the 20 cm^{-1} window above D_0.

During the course of this study the toolbox of the GENIUSH code[50,51,57,58] was extended with the complex absorbing potential (CAP) technique,[59,60] allowing the computation of resonance states. Details about this GENIUSH-CAP approach will be given in a separate publication,[61] here only a couple of important features of the technique are mentioned. The GENIUSH-CAP procedure involves the perturbation of the rovibrational Hamiltonian with a complex potential, thereby making the resonance eigenfunctions square integrable so that they can be expanded in the L^2 basis of the bound states and the eigenstates

Table 2 Experimental (exp) vibrational energy levels of $Ar{\cdot}NO^+$ and their computed counterparts, in cm^{-1}, obtained with the VM, the GENIUSH (GEN), and the close coupling scattering (CC) techniques in reduced (2D) and full (3D) dimensions, relative to the ZPVE. n_s and n_b denote the experimentally determined[26,33] stretching and bending quantum numbers, respectively

	2D		3D			Experiment		
No.	E_{VM}	E_{GEN}	E_{VM}	E_{CC}	E_{GEN}	E_{exp}	n_s	n_b
1	0.0	0.0	0.0	0.0	0.0	0.0	0	0
2	78.2	78.2	78.5	78.5	78.5	79 ± 2	0	1
3	95.9	95.9	96.8	96.8	96.8	94 ± 2	1	0
4	151.2	151.3	152.3	152.3	152.3	155 ± 2	0	2
6	178.5	178.6	179.6	179.6	179.6	178 ± 2	2	0
9	233.2	233.3	234.7	234.6	234.7	230 ± 2	0	3
10	254.3	254.4	255.5	255.5	255.5	256 ± 2	3	0
16	327.3	327.5	328.9	328.8	328.9	328 ± 2	4	0
23	395.9	396.0	397.4	397.4	397.4	391 ± 2	5	0
29		439.6		441.0	441.1	440 ± 2	0	6
30		445.3		446.6	446.7	451 ± 2	6	0
38		488.8		490.3	490.4	484 ± 2	1	5
40		502.5		503.7	503.7	500 ± 2	0	7
41		504.1		505.5	505.6	509 ± 2	7	0
47		536.9		538.3	538.4	531 ± 2	6	1
49		544.6		546.1	546.2	541 ± 2	1	6
51		556.8		557.9	558.0	558 ± 2	0	8
58		585.8		587.2	587.3	583 ± 2	7	1
61		597.1		598.8	598.9	596 ± 2	1	7
64		610.0		611.4	611.5	609 ± 2	0	9
70		631.7		633.1	633.2	631 ± 2	8	1
78		660.7		661.9	661.9	656 ± 2	10	0
85		683.0		684.8	684.9	680 ± 2	9	1
92		705.9		707.3	707.5	700 ± 2	11	0
97		718.5		720.0	720.1	722 ± 2	10	1

with energies above dissociation, computed with GENIUSH. The modified Hamiltonian is

$$\hat{H}'(\eta) = \hat{H} - \eta i W(R), \quad (1)$$

where $\hat{H}$ is the original and $\hat{H}'$ is the complex rovibrational Hamiltonian, η is the CAP-strength parameter, i is the imaginary unit, and $W(R)$ is a real-valued function of the dissociation coordinate R assuming nonzero values at the asymptotic region of the PES. The eigenvalues of the complex matrix are obtained, in atomic units, in the form of $E_0 - i\frac{\Gamma}{2}$, where E_0 is the resonance position and Γ^{-1} is the lifetime of the resonance state. By varying the CAP-strength parameter, eigenvalue trajectories in the complex plane are obtained. Cusps within the trajectories are then detected and associated with resonance positions and lifetimes.

During the GENIUSH-CAP computations, the range of R where the CAP, taken from ref. 62 with polynomial orders of 1, 2, 3, and 5, is turned on is varied between 15 and 50 a_0. The GENIUSH-CAP computations reported utilized 15 and 100 grid points along the r and θ coordinates, respectively, and 100–250 grid points along R. Resonance energies are expected to be accurate to better than 0.1 cm^{-1}, while lifetimes are thought to be computed within 5–25% of their exact values.

Table 3 GENIUSH vibrational energies corresponding to the NO^+ stretching motion obtained using 1D (R and θ fixed to their equilibrium values) and 3D models, in cm^{-1} (no. 2036, for example, refers to the 2036th eigenvalue)

1D		3D	
No.	Value	No.	Value
2	2337.1	2036	2338.2
3	4641.6	5170	4643.4
4	6912.8	8410	6914.9
5	9156.5	11726	9158.5

2.2.2 Close-coupling computations. Details about the close-coupling (CC) computations performed in this study, utilizing the Newmat code,[63] can be found in ref. 37. The propagation along R is performed using the log derivative propagator[64] and a step size of 0.01 a_0. The minimum and maximum propagation distances used are 4.0 and 50.0 a_0, respectively. While in ref. 37 only vibrational states have been computed with the CC technique, in this study rovibrational ($J = 1$ and 2) states have also been obtained. The Newmat code has also been used to perform bound-state computations, denoted here, following ref. 37, as VM. The VM computations are performed using a Chebyshev DVR grid of 500 points in the range of [4.0,50.0] a_0 for R and 14 Gauss–Hermite points in the range of [1.658,2.367] a_0 for r, along with 30 rotational basis functions for NO^+ and a set of 20 Legendre polynomials for the expansion of the angular potential.

Fig. 2 illustrates the partial wave expansion of the rotational quenching cross section of NO^+ ($v = 0, j = 1$) in collision with Ar as a function of the collision energy. Clearly, what appears to be a resonance for a given partial wave may have no effect on the cross section summed over all the partial waves. The situation is even more complex for elastic cross sections. Thus, we compare only the profile of the cross sections with the positions of the resonances obtained with GENIUSH-CAP. In order to facilitate the direct comparison between the GENIUSH-CAP and the close coupling Newmat resonance computations, we also

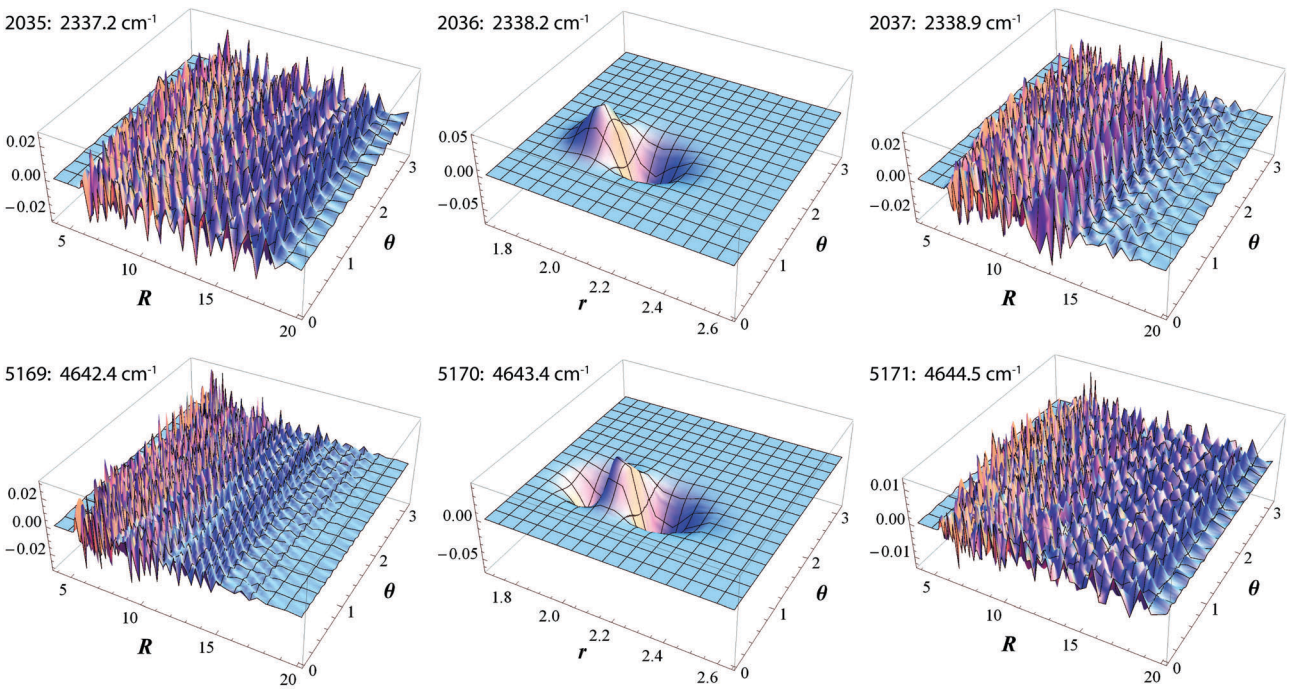

Fig. 3 Plots of the full-dimensional eigenfunctions of the NO^+ stretching fundamental and its first overtone (in the middle of the figure, r–θ cuts), as well as the preceding and subsequent wavefunctions of the system (R–θ cuts).

computed the eigenvalues of the close-coupling Smith lifetime matrix[65] following the method presented previously[66] and compared them to the lifetime values obtained from GENIUSH-CAP computations.

3 Results and discussion

3.1 Variational *vs.* scattering bound-state computations

A comparison of selected bound-state energies computed with GENIUSH (E_{GEN}) and scattering theory (E_{CC}), the latter using only the full Hamiltonian, is shown in Table 1. The complete set of vibrational and rovibrational energy values computed with GENIUSH and scattering theory is given in the ESI.† The agreement between the bound-state energies of the fundamentally different variational and scattering approaches is excellent.

3.2 Bound rovibrational energies

Vibrational progressions of the Ar·NO^+ complex have been measured in the [0,400] and [330,720] cm^{-1} intervals by Takahashi[26] and Bush *et al.*,[33] respectively. The discussion of ref. 37 about the correspondence between some of the experimental[26,33] and computed vibrational energies is extended here to higher energies (see Table 2).

Quantum number assignments are only given in Table 2 for the experimental results, taken from the original references.[26,33] The reason is as follows. Though we attempted to assign quantum numbers to the bound vibrational states *via* the node-counting technique (the bound vibrational wave functions are plotted in Fig. S1–S200 of the ESI†), inspection of the wave-function plots revealed pronounced mixing of the motions along the stretching R and the bending θ coordinates from the very beginning. Assigning stretching (n_s) and bending (n_b) quantum numbers to the computed states is thus rather ambiguous in almost all cases. Furthermore, the stretching and bending progressions "established" experimentally cannot be clearly followed. While a qualitative interpretation of the measured progressions appears to be challenging, the computed vibrational energies do support the observed transitions in an almost quantitative way, see Table 2.

The $J = 1$ and 2 rovibrational energies suggest that while the Ar·NO^+ complex is characterized by two large-amplitude, significantly mixed vibrational motions, the complex rotates basically as a rigid rotor. This is due to the large masses of the nuclei, resulting in rotational constants of only $A_e = 2.4$ and $B_e \approx C_e = 0.1$ cm^{-1}, about two orders of magnitude smaller than the first vibrational excitation energy at 78.5 cm^{-1}.

3.3 On the accuracy of reduced-dimensional treatments

Rovibrational ($J = 0$, 1, and 2) energies obtained with the 2D reduced-dimensional rigid monomer approximation (RMA) model are compared to their full-dimensional counterparts in Tables 1 and 2. The 2D results capture more than the essential physics of the nuclear dynamics: the deviations between the 2D and 3D energies are between 1 and 3 cm^{-1}, never larger than 3 cm^{-1} up to 500 cm^{-1}. Nearer to dissociation, elimination of the NO^+ stretching motion from the dynamical computation causes somewhat more significant differences. The energies increase upon extension from a 2D to a 3D treatment of the vibrations. This is the result of the coupling with the NO^+ stretching fundamental, occurring at about 2340 cm^{-1}, embedded in the dissociation continuum (see Table 3). We can conclude that the RMA model works very well, *i.e.*, the 2D results are almost of spectroscopic accuracy (defined as 1 cm^{-1}).

3.4 Vibrational resonances

3.4.1 Stabilization-method (SM) analysis. The SM histogram of Fig. 1 contains one of the most interesting qualitative results of this study, it provides an overview of the computed eigenvalues of the Ar·NO^+ complex between 0 and 8000 cm^{-1}.

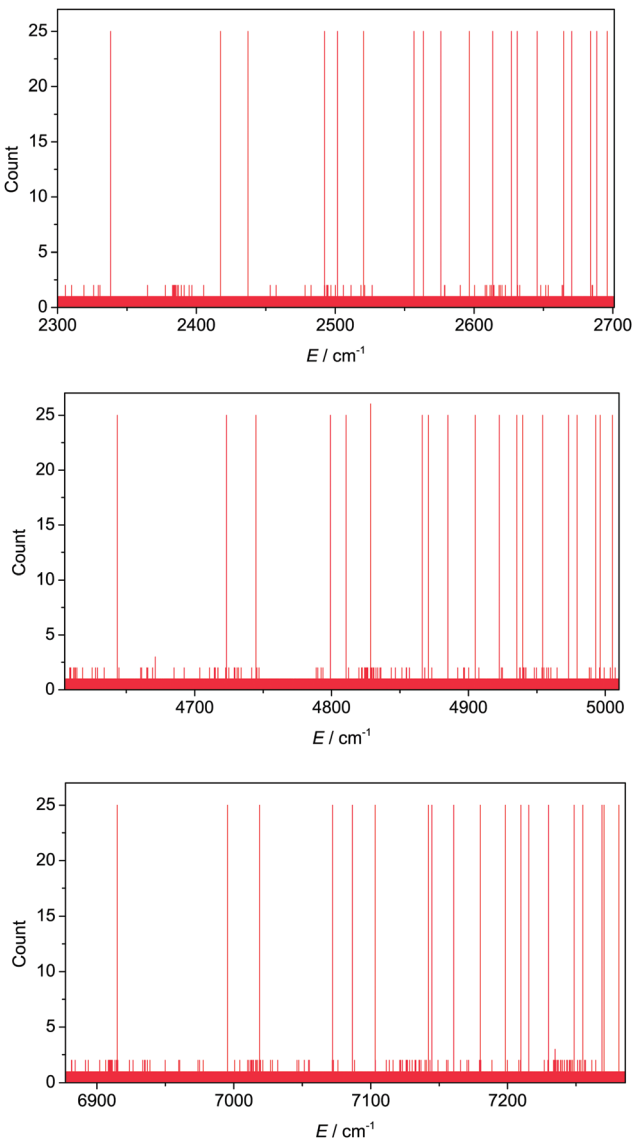

Fig. 4 Stabilization-method histograms covering 400 cm^{-1} above the NO^+ stretch fundamental (top panel) and its first (middle panel) and second (bottom panel) overtones, obtained with 25 GENIUSH computations. All of the panels show 19 long-lived resonances.

The states with green color at the left of the figure correspond to bound states, they show the first dissociation limit, D_0, in a clear and well-defined way. The three further stacks between 2300–3200, 4600–5500, and 6900–7800 cm^{-1} exhibit considerable similarity with the stack corresponding to the bound states. They start at the first, second, and third excited NO^+ stretch states and the width of the stacks is approximately D_0. These observations correspond to a very simple physical picture, namely the nearly ideal adiabatic separation of the small-amplitude NO^+ stretch motion from the other two, large-amplitude, inter-monomer motions.

We can investigate the NO^+ stretch motion further (see Table 3 and Fig. 3 and 4). The zero-point vibrational energy (ZPVE) of Ar·NO^+ is 1278.2 cm^{-1}, while it is 1181.1 cm^{-1} for the 1D diatomic NO^+ model (R and θ are fixed at their equilibrium values). This means that most of the ZPVE is in the diatomic fragment, while the other two, large-amplitude motions contribute less than 100 cm^{-1} to the ZPVE of the Ar·NO^+ complex (in fact, the ZPVE of the 2D RMA model is 96.6 cm^{-1}, showing the almost perfect 1D + 2D additivity of the 3D ZPVE). The bound-state stretch-only 1D vibrational energies of the NO^+ fragment are 2337.1, 4641.6, 6912.8, and 9156.5 cm^{-1} (Table 3),

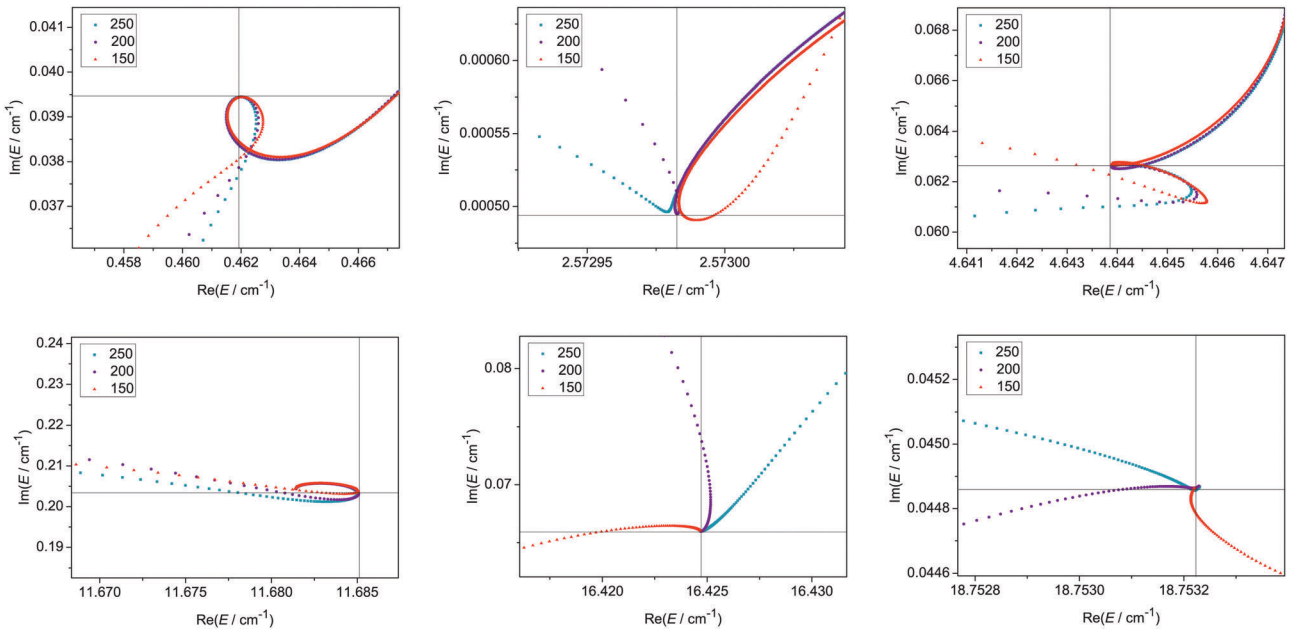

Fig. 5 GENIUSH-CAP eigenvalue trajectories representing six selected resonances in the energy region right above D_0 = 887.00 cm^{-1}. The zero of energy is taken for Ar far from NO^+ (v = 0,j = 0). The CAP eigenvalue trajectories are obtained using computations performed with three different number of DVR points, 150, 200, and 250, along the R dissociation coordinate. Intersections of the horizontal and vertical lines denote the cusps.

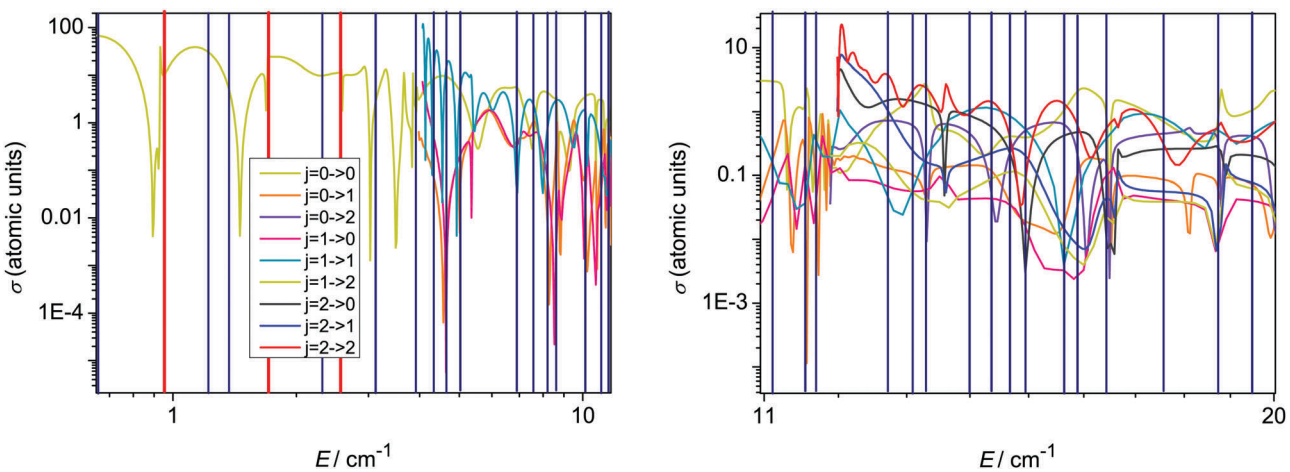

Fig. 6 J = 0 component of the j = 0, 1, 2 → j' = 0, 1, 2 cross sections as a function of the total energy. Blue vertical lines denote energies at which resonances are found in GENIUSH-CAP computations. The red vertical lines emphasize the large peaks of the stabilization method histogram of Fig. 7. The zero of energy is taken for Ar far from NO^+ (v = 0,j = 0).

agreeing very well with the 3D results. Plots corresponding to the 3D wave functions of the NO^+ stretch fundamental and its first overtone are presented in Fig. 3, demonstrating the sharp differences between the wave functions corresponding to the NO^+ stretch motion and those of the neighboring "continuum" states.

In order to have a clearer picture of the resonance states starting with $\nu_r \equiv \nu(NO^+$ stre), $2\nu_r \equiv 2\nu(NO^+$ stre), and $3\nu_r \equiv 3\nu(NO^+$ stre), we present three SM histograms, Fig. 4, showing the first 19 resonances on top of ν_r, $2\nu_r$, and $3\nu_r$, respectively, all in a 400 cm^{-1} interval. The highly similar intermonomer stretching and bending excitations on the adiabatically separated ν_r, $2\nu_r$, and $3\nu_r$ states are clearly visible.

In summary, the SM technique is very successful in identifying the characteristic energy pattern of (long-lived) quasibound states of this complex. This clear pattern and the straightforward energy analysis, using the simplest form of the SM technique, has been possible because of the adiabatic separation of the NO^+-stretching coordinate from the other internal degrees of freedom of the complex.

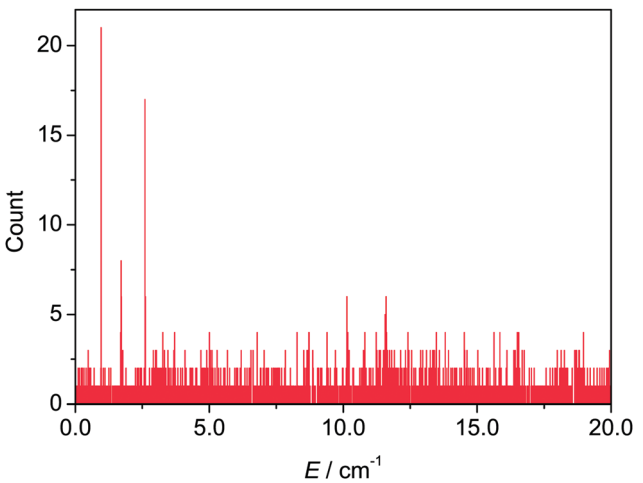

Fig. 7 Stabilization-method (SM) histogram, bin size of 0.01 cm^{-1}, of the energy range 20 cm^{-1} above the first dissociation limit, D_0. The eigenvalues are obtained from 25 GENIUSH computations.

3.4.2 GENIUSH-CAP and scattering results. The GENIUSH-CAP computations give directly, for a given value of J, the total energies and widths of the resonances relative to a zero of the energy associated with Ar far from NO^+ in its ground vibrational and rotational state. Fig. 5 shows a few selected GENIUSH-CAP eigenvalue trajectories with various forms of cusps. The three different colors used in Fig. 5 indicate three different basis sets used along R reflecting convergence of the resonance energies and lifetimes graphically. These computations include all the possible values of j and l such that $|j - l| \leq J \leq j + l$.

In the case of the CC computations, for a given total energy of the $Ar{\cdot}NO^+$ system and for a given value of J and of the parity ε, state to state inelastic cross sections are obtained for all the transitions between the populated rovibrational states of NO^+. The cross sections are illustrated in Fig. 6 for the low-lying vibrational resonances of the $Ar{\cdot}NO^+$ complex. Consequently, this figure shows not only the $0 \rightarrow j$ inelastic cross sections but also cross sections issued from the $j = 1$ and 2 rotational states, which also open in the [0–20] cm^{-1} energy interval represented. In Fig. 6 the GENIUSH-CAP resonance energies are denoted by vertical blue lines, while the energy positions and widths of the peaks of the state to state cross sections drawn as a function of energy define roughly the CC resonance energies and width. When comparing the CC and GENIUSH-CAP results of this figure, one can observe that all significant CC peaks have a GENIUSH-CAP counterpart within a few 0.1 cm^{-1} (the expected agreement of the results obtained with the two techniques).

Experimental cross sections result from the addition of many partial wave contributions, while only a few of these partial waves are participating in a given resonance. The profile of a single partial wave resonance would need to be fitted to a Breit–Wigner form in order to extract the resonance energy and width, which even in this case will differ slightly from the apparent position and width of the peaks of Fig. 6. In the case of $Ar{\cdot}NO^+$, where many partial waves are participating in a state-to-state inelastic cross section, the direct comparison becomes tedious even for the lowest-lying resonances.

To gain further insight into some low-lying resonances, resonances were computed in the region up to 20 cm^{-1} above

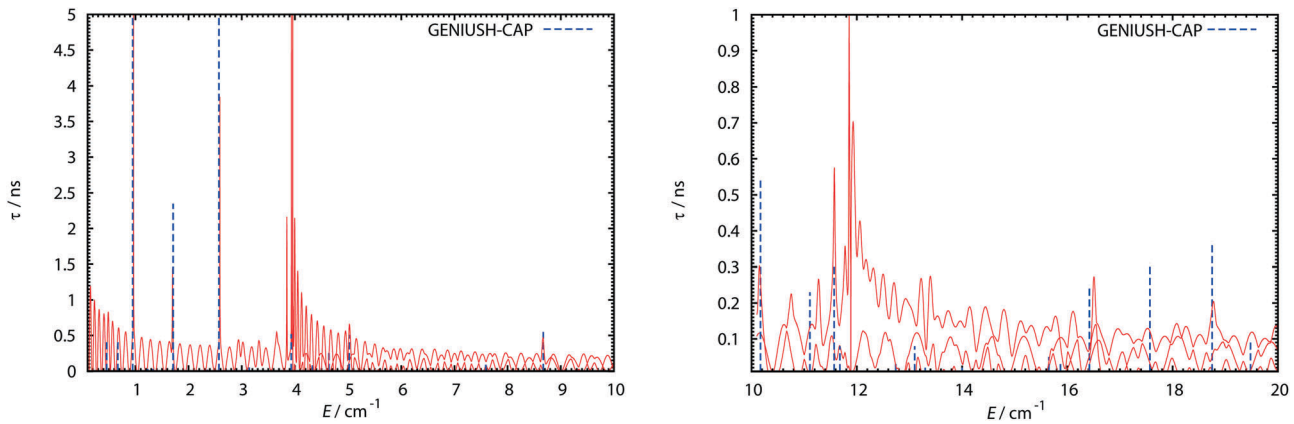

Fig. 8 Comparison between the $J = 0$ resonance energies and lifetimes determined with GENIUSH-CAP and those obtained from close-coupling scattering computations. The zero of energy is taken for Ar far from NO^+ ($v = 0, j = 0$).

D_0 by the stabilization method. We performed 25 standard (Hermitian) GENIUSH computations with different R_{max} values. In the stabilization histogram, shown in Fig. 7, we can easily spot a few stabilized energies, which correspond to "long-lived" resonance states. These resonances have been confirmed by GENIUSH-CAP computations as states with long lifetimes when compared to the other resonance states in this region. These long-lived resonance states found using the SM method are highlighted in red in Fig. 6. The resonance states at 3.9 and 11.6 cm^{-1} are identified with the opening of the $j = 1$ and 2 channels, which occur at 3.9 and 11.9 cm^{-1}, respectively. Other Feshbach resonances can easily be identified, remembering that all the resonances appearing on the $J = 0$ component of the inelastic cross sections starting from the rotational state $j = 0$ of NO^+ are associated with $l = 0$ and are then Feshbach resonances.

We complemented this comparison between the GENIUSH-CAP and CC resonance computations by using the Smith lifetime matrix,[65] which is also a very efficient tool to identify resonances. We take advantage of a Magnus propagator, allowing propagation of an analytical derivative of the scattering matrix as a function of collision energy.[66] The lifetimes obtained as eigenvalues of the close-coupling Smith lifetime matrix are compared with the GENIUSH-CAP lifetimes in Fig. 8. As seen there, the positions of the longest-lived resonances determined with the two different methods are in good agreement, showing again that the two basically different approaches provide results in good agreement not only for the bound but also for the resonance states.

4 Summary and conclusions

The rich internal dynamics of the van der Waals complex of an Ar atom and an NO^+ cation has been studied with a variety of quantum chemical bound, resonance, and scattering techniques employing an accurate potential energy surface[37] representing the ground electronic state. The close-coupling scattering and GENIUSH computations, the latter with the stabilization method and a CAP extension, complement each other and where their results overlap they show excellent numerical agreement.

The PES employed in this study supports 200 bound vibrational states. The internal dynamics of the $Ar{\cdot}NO^+$ complex is determined by the almost perfect adiabatic separation of the stretching of the NO^+ moiety, with the fundamental already beyond the first dissociation limit, from the other two strongly coupled internal degrees of freedom. This separation is manifested not only in the accuracy of reduced-dimensional (rigid monomer) bound-state computations but also in almost perfectly repeated (quasi-bound) energy-level patterns embedded in the dissociation continuum. We have successfully identified several vibrational resonances in the energy region 20 cm^{-1} above the first dissociation threshold using the variational and CC techniques.

Agreement of the computed vibrational energies with the limited experimental information available in the 0–720 cm^{-1} region confirms the accuracy of the PES employed. The observed experimental vibrational progressions are confirmed but their assignment and thus their true physical nature is more subtle than suggested in the experimental studies.[26,33]

There appears to be no experimental high-resolution spectroscopic work on $Ar{\cdot}NO^+$. It is hoped that the present detailed study stimulates such investigations, yielding accurate rotational–vibrational energy levels below and well above the first dissociation asymptote. It is noted in this respect that despite the fact that $Ar{\cdot}NO^+$ exhibits two large-amplitude vibrational motions, the rovibrational states, at least for $J = 1$ and 2, can be described within the standard rigid-rotor approximation.

Acknowledgements

The work performed by A. G. C. received support from NKFIH (grant no. K119658). A. G. C. is also grateful to Université Paris Est for a visiting professorship. E. M. thanks the financial support of a PROMYS grant (no. IZ11Z0_166525) of the Swiss National Science Foundation. J. S. received support from the ÚNKP-16-3 New National Excellence Program of the Ministry of Human Capacities of Hungary. M. H. thanks the French program Physique et Chimie du Milieu Interstellaire (PCMI) funded by the Conseil National de la Recherche Scientifique (CNRS) and the Centre National d'Etudes Spatiales (CNES). The authors gratefully acknowledge the support of the COST Action CM1405 entitled MOLIM: Molecules in Motion. Computer time for some of the quantum dynamics computations was provided by the Mesocentre de Calcul Intensif Aquitain computing facilities of the Université de Pau et des Pays de l'Adour. The authors are grateful to Professor Bill Poirier for a number of useful comments on the manuscript.

References

1 *Dynamics of polyatomic van der Waals complexes*, ed. N. Halberstadt and K. C. Janda, Plenum, New York, 1990, vol. 227.
2 M. C. Heaven, *Annu. Rev. Phys. Chem.*, 1992, **43**, 283.
3 A. Rohrbacher, N. Halberstadt and K. C. Janda, *Annu. Rev. Phys. Chem.*, 2000, **51**, 405.
4 D. S. Boucher and R. A. Loomis, *Adv. Chem. Phys.*, 2008, **138**, 375.
5 J. A. Beswick, N. Halberstadt and K. C. Janda, *Chem. Phys.*, 2012, **399**, 4.
6 G. Quéméner and P. S. Julienne, *Chem. Rev.*, 2012, **112**, 4949–5011.
7 B. Yang and B. Poirier, *J. Phys. B: At., Mol. Opt. Phys.*, 2012, **45**, 135102.
8 M. Dubernet, M. Alexander, Y. Ba, N. Balakrishnan, C. Balança, C. Ceccarelli, J. Cernicharo, F. Daniel, F. Dayou and M. Doronin, *et al.*, *Astron. Astrophys.*, 2013, **553**, 50.
9 M. J. Barlow, *Science*, 2013, **342**, 1343.
10 R. A. Theis, W. J. Morgan and R. C. Fortenberry, *Mon. Not. R. Astron. Soc.*, 2015, **446**, 195.
11 Y. Xiao and B. Poirier, *J. Phys. Chem.*, 2006, **110**, 5475–5480.
12 J. Tennyson and B. T. Sutcliffe, *J. Chem. Phys.*, 1983, **79**, 43.

13 H.-J. Werner, B. Follmeg, M. H. Alexander and D. Lemoine, *J. Chem. Phys.*, 1989, **91**, 5425.
14 A. Bergeat, J. Onvlee, C. Naulin, A. van der Avoird and M. Costes, *Nat. Chem.*, 2015, **7**, 349.
15 J. Tennyson and B. T. Sutcliffe, *J. Chem. Phys.*, 1982, **77**, 4061.
16 A. R. W. McKellar, *J. Chem. Phys.*, 1988, **88**, 4190.
17 A. G. Ayllon, J. Santamaria, S. Miller and J. Tennyson, *Mol. Phys.*, 1990, **71**, 1043.
18 R. Prosmiti, P. Villarreal and G. Delgado-Barrio, *Chem. Phys. Lett.*, 2002, **359**, 473.
19 A. Valdés, R. Prosmiti, P. Villarreal, G. Delgado-Barrio, D. Lemoine and B. Lepetit, *J. Chem. Phys.*, 2007, **126**, 244314.
20 R. Prosmiti, C. Cunha, P. Villarreal and G. Delgado-Barrio, *J. Chem. Phys.*, 2003, **119**, 4216.
21 P. R. R. Langridge-Smith, E. M. Carrasquillo and D. H. Levy, *J. Chem. Phys.*, 1981, **74**, 6513.
22 P. D. A. Mills, C. M. Western and B. J. Howard, *J. Phys. Chem.*, 1986, **90**, 3331.
23 O. L. A. Monti, H. A. Cruse, T. P. Softley and S. R. Mackenzie, *Chem. Phys. Lett.*, 2001, **333**, 146.
24 W. D. Rellergert, S. T. Sullivan, S. J. Schowalter, S. Kotogichova, K. Chen and E. R. Hudson, *Nature*, 2013, **495**, 490–494.
25 T. Stoecklin, P. Halvick, M. A. Gannaouni, M. Hochlaf, S. Kotochigova and E. R. Hudson, *Nat. Commun.*, 2016, **7**, 11234.
26 M. Takahashi, *J. Chem. Phys.*, 1992, **96**, 2594–2599.
27 J.-M. Robbe, M. Bencheikh and J.-P. Flament, *Chem. Phys. Lett.*, 1993, **210**, 170.
28 K. Sato, Y. Achiba and K. Kimura, *J. Chem. Phys.*, 1984, **81**, 57.
29 T. G. Wright, V. Špirko and P. Hobza, *J. Chem. Phys.*, 1994, **100**, 5403.
30 I. Fourré and M. Raoult, *Chem. Phys.*, 1995, **199**, 215.
31 T. G. Wright, *J. Chem. Phys.*, 1996, **105**, 7579.
32 A. M. Bush, T. G. Wright, V. Špirko and M. Juřek, *J. Chem. Phys.*, 1997, **106**, 4531.
33 A. M. Bush, J. M. Dyke, P. Mack, D. M. Smith and T. G. Wright, *J. Chem. Phys.*, 1998, **108**, 406.
34 J. D. Barr, J. M. Dyke, P. Mack, D. M. Smith and T. G. Wright, *J. Electron Spectrosc. Relat. Phenom.*, 1998, **97**, 159.
35 M. C. R. Cockett, K. Müller-Dethlefs and T. G. Wright, *Annu. Rep. Prog. Chem., Sect. C: Phys. Chem.*, 1998, **94**, 327.
36 E. P. F. Lee, P. Soldán and T. G. Wright, *J. Phys. Chem. A*, 1998, **102**, 6858.
37 P. Halvick, T. Stoecklin, F. Lique and M. Hochlaf, *J. Chem. Phys.*, 2011, **135**, 044312.
38 R. Linguerri, N. Komiha and M. Hochlaf, *Phys. Chem. Chem. Phys.*, 2012, **14**, 4236.
39 Y. Tebai, N. Jaidane, D. Ben Abdallah, P. Halvick and T. Stoecklin, *J. Chem. Phys.*, 2014, **141**, 174305.
40 K. T. Giju, S. Roszak and J. Leszczynski, *J. Chem. Phys.*, 2002, **117**, 4803.
41 G. E. Froudakis, G. S. Fanourgakis, S. C. Farantos and S. S. Xantheas, *Chem. Phys. Lett.*, 1998, **294**, 109.
42 P. Zhang, Y. Zhao, F. Hao, X. Song, G. Zhang and Y. Wang, *J. Mol. Struct.: THEOCHEM*, 2009, **899**, 111.
43 T. Ritschel, P. J. Kuntz and L. Zülicke, *Eur. Phys. J. D*, 2007, **44**, 93.
44 D. T. Anderson, S. Davis and D. J. Nesbitt, *J. Chem. Phys.*, 1997, **107**, 1115.
45 N. I. Hammer, E. G. Diken, J. R. Roscioli, M. A. Johnson, E. M. Myshakin, K. D. Jordan, A. M. McCoy, X. Huang, J. M. Bowman and S. Carter, *J. Chem. Phys.*, 2005, **122**, 244301.
46 A. G. Császár, *Wiley Interdiscip. Rev.: Comput. Mol. Sci.*, 2012, **2**, 273–289.
47 H. H. Nielsen, *Rev. Mod. Phys.*, 1951, **23**, 90.
48 I. M. Mills, *Molecular Spectroscopy: Modern Research*, 1972.
49 A. G. Császár, C. Fábri, T. Szidarovszky, E. Mátyus, T. Furtenbacher and G. Czakó, *Phys. Chem. Chem. Phys.*, 2012, **14**, 1085–1106.
50 E. Mátyus, G. Czakó and A. G. Császár, *J. Chem. Phys.*, 2009, **130**, 134112.
51 C. Fábri, E. Mátyus and A. G. Császár, *J. Chem. Phys.*, 2011, **134**, 074105.
52 A. U. Hazi and H. S. Taylor, *Phys. Rev. A: At., Mol., Opt. Phys.*, 1970, **1**, 1109–1120.
53 V. A. Mandelshtam, T. R. Ravuri and H. S. Taylor, *Phys. Rev. Lett.*, 1993, **70**, 1932–1935.
54 A. Riera, *J. Phys. Chem.*, 1993, **97**, 1558–1565.
55 J. Müller, X. Z. Yang and J. Burgdorfer, *Phys. Rev. A: At., Mol., Opt. Phys.*, 1994, **49**, 2470–2475.
56 E. Mátyus, *J. Phys. Chem. A*, 2013, **117**, 7195.
57 E. Mátyus, C. Fábri, T. Szidarovszky, G. Czakó, W. D. Allen and A. G. Császár, *J. Chem. Phys.*, 2010, **133**, 034113.
58 C. Fábri, E. Mátyus and A. G. Császár, *Spectrochim. Acta, Part A*, 2014, **119**, 84–89.
59 U. V. Riss and H. D. Meyer, *J. Phys. B: At., Mol. Opt. Phys.*, 1993, **26**, 4503–4536.
60 H. Y. Mussa and J. Tennyson, *Chem. Phys. Lett.*, 2002, **366**, 449–457.
61 D. Papp, T. Szidarovszky, K. Yamanouchi and A. G. Császár, *J. Chem. Phys.*, 2017, to be submitted.
62 B. Poirier and T. Carrington, *J. Chem. Phys.*, 2003, **118**, 17–28.
63 T. Stoecklin, A. Voronin and J. C. Rayez, *Phys. Rev. A: At., Mol., Opt. Phys.*, 2002, **66**, 042703.
64 D. E. Manolopoulos, PhD thesis, University of Cambridge, 1988.
65 F. T. Smith, *Phys. Rev.*, 1960, **118**, 349–356.
66 G. Guillon and T. Stoecklin, *J. Chem. Phys.*, 2009, **130**, 144306.

